ACS OMEGA

http://pubs.acs.org/journal/acsodf

Article

A Comparative Investigation of Chemically Reduced Graphene Oxide Thin Films Deposited via Spray Pyrolysis

Ilhem Bargaoui, Nabila Bitri,* and Jean-Michel Ménard*

Cite This: *ACS Omega* 2022, 7, 11973−11979

Read Online

ACCESS | Metrics & More | Article Recommendations

ABSTRACT: We present a comparative investigation between thin films of graphene oxide (GO) and chemically reduced graphene oxide (rGO) deposited onto glass substrates via spray pyrolysis. Two reduction techniques are investigated: (1) the exposition of a sprayed layer of GO to vapors of hydrazine hydrate to produce rGO_V and (2) the addition of liquid hydrazine hydrate to a suspended GO solution, which is then sprayed onto a substrate to produce rGO_L. Three different spectroscopy techniques, Raman, Fourier transform infrared, and UV−Vis−NIR, show that the two reduced samples have less lattice disorder in comparison to GO, with rGO_L having the highest degree of reduction. Interestingly, topography characterization by atomic force microscopy reveals a morphological change occurring during the exposure to hydrazine hydrate vapors, resulting in a thickness of 110 nm for the rGO_V film, which is a factor of 16 larger than rGO_L and GO. Finally, *I*−*V* measurements show a significant decrease of the GO's resistivity after the reduction process, where rGO_L features a resistivity 90 times lower than rGO_V, confirming that rGO_L has the highest degree of reduction. Our results indicate that the reduction process for rGO_V is susceptible to introducing intercalated water molecules in the material while the fabrication technique for rGO_L is a suitable route to obtain a material with minimal lattice disorder and properties approaching those of graphene.

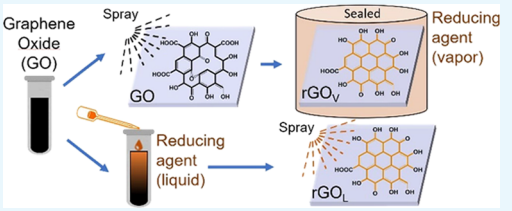

Downloaded via 174.119.148.7 on June 14, 2022 at 04:00:47 (UTC).
See https://pubs.acs.org/sharingguidelines for options on how to legitimately share published articles.

INTRODUCTION

Graphene oxide (GO) has received considerable interest from researchers due to its ease of fabrication from carbon and its dispersibility in liquid water. Thus, these materials can be fabricated via a low-cost scalable wet chemistry technique,[1−3] enabling fast deposition processes such as drop-casting,[4] dip casting,[2] and spray pyrolysis.[5] Different fabrication and deposition approaches offer several paths to control the degree of reduction of GO[6] and effectively functionalize it by decreasing the level of oxidation and creating a material closer in composition and properties to graphene.[7,8] Reduction techniques can rely on thermal annealing,[9] laser illumination,[10] or exposure to a chemical reducing agent such as hydrazine hydrate.[11] They can also involve different functional materials such as nanoparticles,[12] organic compounds,[13] polymers,[14] and biomaterials,[15] which also affect the material properties.

As a result, GO and its reduced form, rGO, exhibit a range of properties that can be optimized for different kinds of applications. For example, they can be used for gas sensing since their electrical conductivity strongly depends on bond chemicals on their surface.[16] They also have high conductivity and a structure that can be made porous to build efficient supercapacitors[17] or enhance the performances of solar cells.[5,18] These graphene-like materials have also found applications in optics due to their nonlinear properties[19,20] and in medicine as a drug release matrix for targeting cancer cells.[21] However, the efficient use of GO and rGO in these applications can be limited by their arbitrary amount of lattice disorder, which is due to several key factors, including the fabrication technique.[22,23] Therefore, a better understanding of the fabrication procedure, including the reduction process, and their effects on the materials' properties is an essential step to enable future GO-based technologies.

Many groups have previously reported different fabrication techniques to reduce GO and performed measurements to demonstrate a decrease in the lattice disorder. For example, Park et al.[24] reported a reduction method to modify colloidal suspensions of GO using different organic systems. To efficiently reduce GO, they added 1 μL of hydrazine hydrate to 3 mg of GO diluted in DMF/H_2O (9:1). They allowed the liquid to dry under an Ar atmosphere at 150 °C and monitor the reduction via the material's conductivity. Youn et al.[25] exposed a GO thin film to hydrazine hydrate vapor, up to 12 h, to obtain rGO, as demonstrated from X-ray photoelectron spectroscopy (XPS), Raman spectra, and optical absorption experiments. Also, Guo et al.[26] used a pulsed laser to induce a reduction of GO, which they monitor by measuring the decrease in bandgap energy from 2.4 to 0.9 eV. Finally, a

Received: January 6, 2022
Accepted: March 16, 2022
Published: March 29, 2022

© 2022 The Authors. Published by American Chemical Society

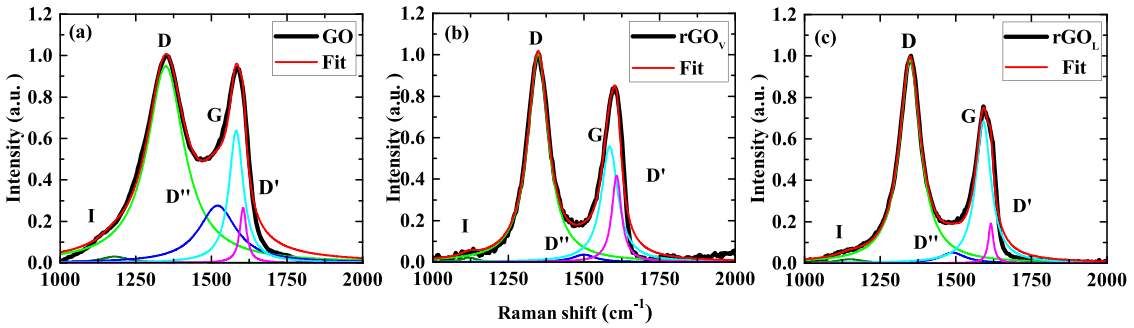

Figure 1. Deconvolution of Raman spectra peaks of (a) GO, (b) rGO_V, and (c) rGO_L thin films deposited via spray pyrolysis at 150 °C.

hydrothermal preparation of rGO powder from a GO solution was reported by Chang et al.[27] In their experiment, the rGO powder is dispersed in ethanol/H_2O (1:1), sonicated, and then drop-cast onto an Al_2O_3 substrate. They measure the current−voltage characteristic to trace a resistivity smaller than GO due to the reduction process.

Here, we produce and characterize GO and rGO thin films sprayed onto a glass substrate. The rGO is fabricated with two chemical reduction methods based on hydrazine hydrate; the first method uses the reducing agent in vapor phase and the second in liquid phase. To our knowledge, this is the first demonstration and study of rGO produced with the second method. We rely on complementary techniques to characterize the samples: Raman spectroscopy and Fourier transform infrared spectroscopy (FTIR) are used to investigate lattice disorder related to the presence of functional groups, optical spectroscopy reveals the bandgap energy, atomic force microscopy (AFM) provides information about the roughness and sample thickness and, finally, *I*−*V* electrical measurements yield information on the sample's conductivity.

RESULTS AND DISCUSSION

The fabrication of GO and rGO thin films uses a nanocolloidal solution of GO in water, which is deposited by spray pyrolysis onto a glass substrate to obtain thin films. The reduction process is carried out following two different approaches. We first expose a GO thin film to hydrazine hydrate vapors at 100 °C, for 24 h, inside a sealed Petri dish. We refer to this sample as rGO_V in relation to the vapor phase (V) of the reducing agent. Then, liquid hydrazine hydrate is added to the original GO solution, which, after 24 h, this solution is similarly deposited on a substrate by spray pyrolysis. Note that no heating or filtering process of the solution is required. We refer to this sample as rGO_L in relation to the liquid phase (L) of the reducing agent.

To investigate the crystallographic structures of our samples, we investigate their vibrational modes with Raman spectroscopy. Figure 1a−c shows the spectra for GO, rGO_V, and rGO_L, respectively. Here, we follow the peaks' nomenclature used in refs 28−30 where the two bands, D and G bands, are deconvoluted into five distinctive peaks. We identify the spectral position of the D and G peaks, indicative of the carbon-like nature of the material, as well as the three additional modes, I, D″, and D′, attributed to the disordered structure. The baseline is corrected using the asymmetric least squares method to remove artifacts, notably due to luminescence.[31] When considering the five Raman resonances mentioned above, the fits are in good agreement with the experimental data. We observe in all samples a large G peak related to sp^2 hybridizations,[32] associated with the graphene honeycomb structure. As expected, the D peak activated by the defects (mainly the epoxy and the hydroxyl groups) is dominant and always present in oxidized graphene.[33] The additional resonances named I, D″, and D′ peaks, which appear in all samples, are also related to the disorder. More particularly, Schwan et al.[34] attributed the I peak to compressive stress in the film while Tanet al.[35] consider that it becomes active when selection rules are relaxed due to the presence of defects. The peak D″ appears because of amorphous sp^2 bonds and interstitial defects,[36] and it can be attributed to the bond disorder caused by the attached functional groups such as −COOH, −COC, and −OH.[37,38] Graphene-like materials generally contain the peak D′ as it is related to an oxidized sp^2 carbon hybridization, resulting in an sp^3 hybridization,[39] but can also be observed for intercalation compounds.[28,40] Although we expect the reduced samples to show a larger proportion of sp^2 hybridization associated with the G peak in the Raman spectrum, we also find the ratio between the D and G peaks to be relatively constant in all three samples. As a result, a more complete analysis comparing all Raman peaks is necessary to confirm chemical changes.[28,29] Both rGO_V and rGO_L show a strong reduction of the D″ peak in comparison to GO as well as a narrower full width at half maximum (FWHM) of the D peak, indicating that the reducing agent effectively removes defects in GO.[6] The increase in the D′ peak in the rGO_V sample indicates that the reducing agent in vapor form interacts preferentially with the surface but less effectively throughout the deposited thin film to remove sp^3 hybridizations, which results in a relatively small creation of new sp^2 hybridization. Partial hydration of the material, which could occur during the reduction process, may contribute to increase the D′ peak amplitude.

Furthermore, we observe an overall narrowing of the bands in the reduced samples in agreement with previous work,[6,41] which indicates an increase in the planar order of graphitic materials.[33] The two rGO samples also exhibit a reduced D″ peak amplitude, indicating less amorphous sp^2 bonds. The precise positions of the I, D, D″, G, and D′ peaks (in increasing order of wavenumber), for the three samples investigated in this work, are listed in Table 1. The peaks D, G, and D′ are found at their expected spectral position.[6,28,32,37] The extracted spectral positions of the I and D″ peaks have the largest uncertainty because of their relatively small amplitude and their large FWHM. We find nonetheless good overall agreement between our results and those reported in previous studies.[28,29]

While Raman spectroscopy provides information about the activated vibration modes in the samples, FTIR directly

https://doi.org/10.1021/acsomega.2c00108
ACS Omega 2022, 7, 11973−11979

Table 1. Raman Resonance Peak Positions for GO, rGO_V, and rGO_L

	peak position (cm^{-1})				
sample	I	D	D″	G	D′
GO	1180	1349	1521	1582	1605
rGO_V	1120	1348	1500	1585	1608
rGO_L	1150	1349	1490	1591	1616

addresses the existence of chemical groups in the material. Figure 2 presents the FTIR spectra of GO (black line), rGO_V (red line), and rGO_L (blue line). The reflection spectra of GO present a dominant peak of C−OH vibration mode (1260 cm^{-1}) and an additional side peak corresponding to C═O (1750 cm^{-1}) of the carbonyl group, indicating a high oxidation degree of the sample. For the two rGO samples, the peak related to C−OH is less intense than the one observed with GO and it disappears almost entirely in the case of rGO_V. We observe instead a dominant peak related to C−O bonds at a slightly lower energy (1085 cm^{-1}). This shifted resonance indicates the effect of a reducing agent acting preferentially on hydrogen bonds, which are easier to reduce than C−O bonds of the epoxide group (C−O−C).[42] The band appearing around 3530 cm^{-1} is usually referred to the stretching mode of the hydroxyl groups O−H. This band is significantly more intense for rGO_V and is likely due to the presence of water molecules. This indicates that water, in vapor form, may be a contaminant during the reduction process performed in a sealed container at 100 °C, especially considering that GO can easily absorb water molecules.[43] For rGO_V and rGO_L, the peak corresponding to inoxidized carbon atoms, C═C, has appeared. The fact that rGO_L has the most pronounced C═C peak (1615 cm^{-1}) indicates that this sample has the highest degree of reduction in our experiment. This result agrees with the conclusions drawn from the Raman measurements. All FTIR spectral peak positions identified in Figure 2 are in good agreement with previous work.[44−47]

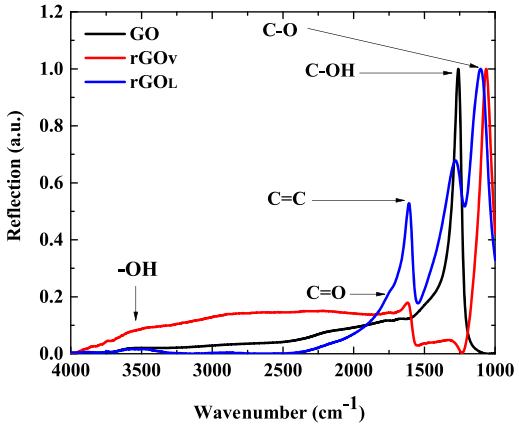

Figure 2. FTIR spectra in reflection mode for GO, rGO_V, and rGO_L thin films deposited via spray pyrolysis at 150 °C.

The oxidation of graphene increases the material's optical bandgap energy E_g. Consequently, one expects the reduction process to decrease the measured bandgap energy since rGO is more graphene-like than GO.[48,49] Figure 3 presents the Tauc plot,[50] which is used to estimate the bandgap values of our samples based on optical reflection experiments and the following expression:[51]

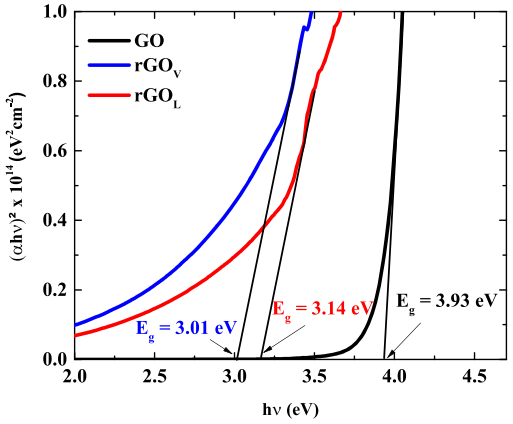

Figure 3. Tauc plots of GO, rGO_V, and rGO_L thin films deposited via spray pyrolysis at 150 °C.

$$\alpha h\nu = A(h\nu - E_g)^n \quad (1)$$

where α is the linear absorption coefficient, A is a constant measuring the disorder of the material,[52,53] h is Plank's constant, ν is the incident photon's frequency, and n is equal to 1/2 since GO and rGO are considered direct bandgap materials.[54,55] From the experimental measurements, we extract E_g = 3.93 eV for GO and lower values of 3.01 and 3.14 eV for rGO_V and rGO_L, respectively. These smaller bandgap energies are consistent with a material structurally closer to graphene. Our results are within the range of energies reported for GO and rGO thin films in previous studies,[49,56] but the induced changes are small in comparison to other work using different reduction methods[26] or studying rGO in a powder state.[48] The measured bandgap energy does not only depend on the degree of reduction but also on the thickness and structural properties of the thin film. As shown below, AFM measurements reveal that the rGO_V sample in this work has a much larger thickness than GO and rGO_L. This difference can explain why rGO_V features the lowest bandgap energy although rGO_L is a more graphene-like material according to Raman and FTIR measurements.

We examined the morphological properties of our samples with AFM. Besides information about the surface roughness and sample uniformity, we also measure the layer thickness, which is indicative of the compactness and porosity of the thin film. Figure 4 presents the AFM micrographs and profile curves of the three samples using the same quantity of dissolved material and the same spray pyrolysis deposition parameters. The darker vertical stripes at the right edge of each image in Figure 4 correspond to the bare substrate. A razor blade is used to remove the graphitic material and obtain this plane of reference, allowing us to precisely measure the thin film thickness with AFM. A micrograph of the GO sample (Figure 4a) shows a relatively uniform film with a roughness of 3.9 nm for an average thickness of 10.8 nm.

The micrograph of the rGO_V sample (Figure 4b) presents a much larger roughness of 55.7 nm with microbubbles, indicating possible detachments of the thin film from the substrate, and a surprisingly large average thickness of 110 nm. This result might be in part attributed to localized hydration of the sample during the reduction process. GO is hydrophilic and its interplanar distance can expand up to 1.2 nm in a water environment.[57,58] Our observations of a microscopically rough surface are consistent with previous work also using reducing

https://doi.org/10.1021/acsomega.2c00108
ACS Omega 2022, 7, 11973−11979

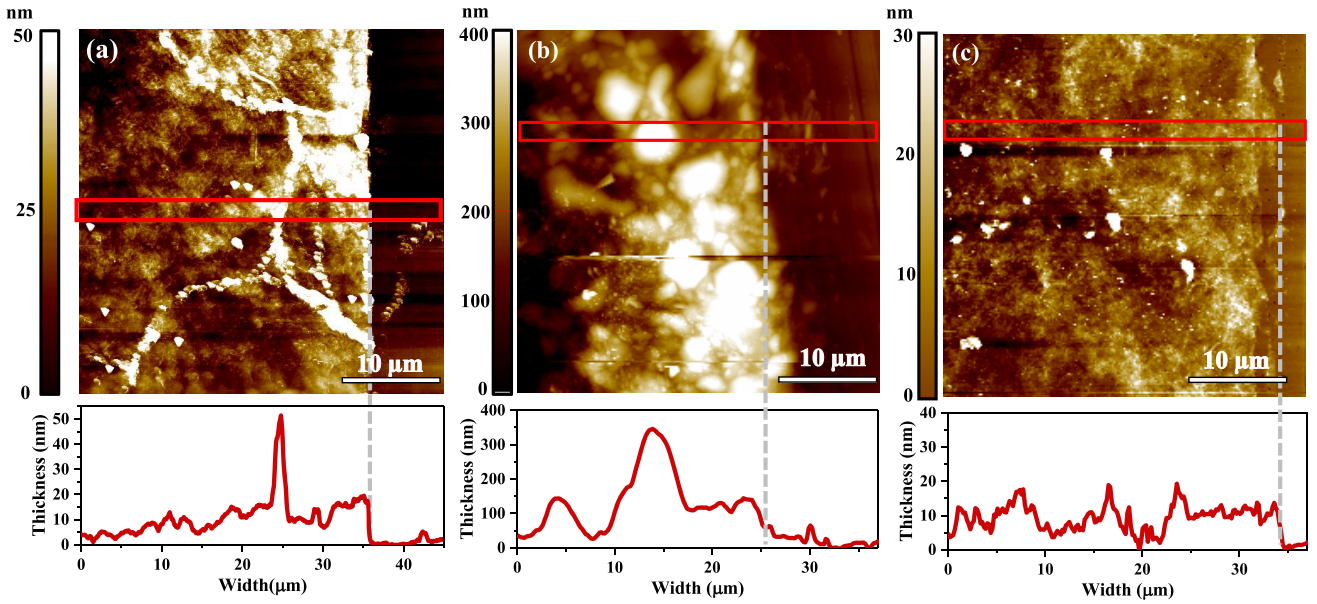

Figure 4. AFM micrographs and profile curves of (a) GO, (b) rGO_V, and (c) rGO_L were used to extract their surface roughness and layer thickness.

agents in the vapor phase.[59] Finally, the micrograph of the rGO_L sample (Figure 4c) shows a much more uniform film, with a roughness of 2.1 nm and thickness of 6.4 nm, comparable to the GO sample. We can conclude that adding a liquid reducing agent to the GO solution before spray pyrolysis deposition leads to a homogeneous reduced material and helps prevent the thin film's surface irregularities. The moderately smaller thickness of the rGO_L in comparison to the GO can be attributed to the reduction process, removing out-of-plane functional groups.[22]

For most applications related to graphitic materials, one of the most important properties of these materials is their electrical resistivity, which can be extracted from the $I-V$ curve. Figure 5 presents the current−voltage behavior of the

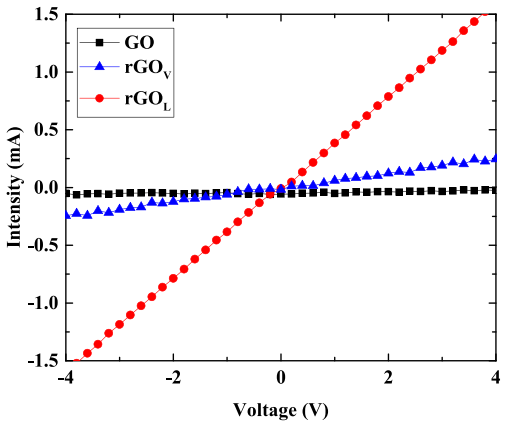

Figure 5. $I-V$ curves of GO, rGO_V, and rGO_L thin films with resistivity values of 300×10^{-3}, 180×10^{-3}, and 2×10^{-3} Ω.cm, respectively.

three samples. The curves show a linear relationship, indicative of an ohmic behavior and an absence of Schottky diode response due to the electrodes.[60,61] The extracted resistance R values of the GO, rGO_V, and rGO_L samples are 280, 16, and 2.5 KΩ, respectively. We use the following relation to extract the resistivity from the measured resistance:[62]

$$\rho = \frac{tL}{d}R \tag{2}$$

where t is the measured thickness of each sample, R is the resistance, L is the length of electrodes, and d is the distance between the electrodes. Both L and d correspond to 1.5 cm in our setup. The extracted resistivity values for GO, rGO_V, and rGO_L are 300×10^{-3}, 180×10^{-3}, and 2×10^{-3} Ω.cm, respectively. As expected, we observe a drop in resistivity after the reduction process. The sample rGO_L displays the lowest resistivity, almost two orders of magnitude smaller than rGO_V, which indicates once more that the reduction technique based on the liquid hydrazine hydrate leads to a higher degree of reduction in comparison to the process relying on the gas phase. The measured resistivity values for both rGO samples are higher than those reported in previous work using high-temperature annealing[63] or hydrothermal fabrication[27] to produce rGO but lower than the resistivity reported by other work using an optical reduction process.[64] Finally, the hot point probe method is used to determine that the holes present the minority carriers, and the electrons form the majority free carrier population in rGO_V and rGO_L. As a result, the electrical properties are mostly determined by electron density and mobility.

CONCLUSIONS

Reduction of graphene oxide has been performed with two different chemical techniques based on hydrazine hydrate in vapor or liquid phase and then deposited by spray pyrolysis to obtain thin film samples, rGO_V and rGO_L, respectively. Raman spectroscopy measurements show that rGO_L exhibits less lattice disorder than rGO_V. The FTIR spectra of rGO_L reveal a more intense inoxidized carbon peak in comparison to rGOv, indicating a better degree of reduction, while rGOv interestingly exhibits a reduced density of C−OH groups. Furthermore, spectrophotometer measurements show that the GO's bandgap decreases from 3.9 to ∼3 eV after the reduction process, indicating a transition from an insulator to a semiconductor state. AFM measurements indicate that the rGO_L film thickness is thinner than the GO film due to the

https://doi.org/10.1021/acsomega.2c00108
ACS Omega 2022, 7, 11973−11979

removal of functional groups, while the rGO_V film, also containing the same amount of original GO material, appears surprisingly thick, a factor of 10 larger than GO, due to the large inhomogeneity and surface roughness. Finally, $I-V$ measurements reveal a significant decrease in the GO's resistivity after reduction, where rGO_L features a resistivity 90 times lower than rGO_V, confirming that rGO_L has the highest degree of reduction. We demonstrate fabrication steps that are simple and scalable to enable GO and particularly rGO to be implemented in a variety of scientific and industrial applications. Our results can lead to different optical, chemical, structural, and electrical properties, with rGO_V partially responsible for partial hydration of the material and rGO_L featuring properties closest to those of graphene.

MATERIALS AND METHODS

Synthesis of Graphene Oxide and Reduced Graphene Oxide Films. The fabrication of GO and rGO thin films used a nanocolloidal solution (5 mL) of GO in H_2O (Sigma Aldrich) diluted to a concentration of 0.5 mg/mL. The solution was ultrasonicated for 30 min at room temperature and deposited by spray pyrolysis onto heated glass substrates at 150 °C with an airbrush (VH174, VIVOHOME) to obtain thin films. To fabricate rGO_V, we exposed a GO thin film to hydrazine hydrate vapors at 100 °C, for 24 h, at a concentration corresponding to 0.1 mL evaporated inside a sealed Petri dish (9 cm diameter, 4 cm height). We fabricated rGO_L using 0.2 mL of liquid hydrazine hydrate, which was added to the original GO solution. After 24 h, the solution was deposited on a substrate with the same spray pyrolysis technique described above.

Material Characterization. Optical and electrical instruments were used to characterize the samples. Raman spectroscopy was performed with a WItec 300RSA confocal system at a wavelength of 532 nm and optical power of 3.6 W to trace vibrational resonances. A Fourier transform infrared FTIR spectrometer (Nicolet) was operated in reflection mode over a spectral range extending from 400 to 4000 cm^{-1} to identify the existing chemical bonds. A UV−Vis−NIR spectrophotometer (SHIMADZU UV-3100S), operating over a wavelength range of 300 to 1800 nm, was used to determine the optical bandgap of the samples. Atomic force microscopy (AFM Park NX 10) was used to study the morphological properties and the thickness of the sample. Two parallel silver paint stripes connected manually by copper wires were used as electrodes to measure the $I-V$ response (Agilent N6700B) and characterize the thin film resistivity. The length of the electrodes (L) and their separation (d) are both 1.5 cm. Finally, the same circuit with an ammeter was used to determine the types of majority charge carriers in our samples using the hot probe method[65] referenced to an n-type Si wafer.

AUTHOR INFORMATION

Corresponding Authors

Nabila Bitri − *National Engineering School of Tunis, Photovoltaic and Semiconductor Materials Laboratory, University of Tunis El Manar, Tunis 1002, Tunisia*; Email: nabila.b.hamdi@gmail.com

Jean-Michel Ménard − *Department of Physics, University of Ottawa, Ottawa, Ontario K1N 6N5, Canada*; orcid.org/0000-0002-6458-758X; Email: jean-michel.menard@uottawa.ca

Author

Ilhem Bargaoui − *Faculty of Sciences of Tunis, University of Tunis El Manar, Tunis 1068, Tunisia; National Engineering School of Tunis, Photovoltaic and Semiconductor Materials Laboratory, University of Tunis El Manar, Tunis 1002, Tunisia; Department of Physics, University of Ottawa, Ottawa, Ontario K1N 6N5, Canada*

Complete contact information is available at: https://pubs.acs.org/10.1021/acsomega.2c00108

Funding

The authors are thankful to the Canadian organization "MITACS" for financial support. J.-M.M. acknowledges funding from the National Sciences and Engineering Research Council of Canada (NSERC).

Notes

The authors declare no competing financial interest.

ACKNOWLEDGMENTS

The authors are grateful to Prof. Wissem Dimassi for the FTIR measurements performed in Energy Research and Technology Center CRTEn, Borj Cedria, Tunisia.

NOMENCLATURE

GO graphene oxide
rGO_V reduced graphene oxide (using a reducing agent in vapor phase)
rGO_L reduced graphene oxide liquid (using a reducing agent in liquid phase)
FTIR Fourier transform infrared
AFM atomic force microscopy
FWHM full width at half maximum

REFERENCES

(1) Ruoff, R. Calling All Chemists. *Nat. Nanotechnol.* **2008**, *3*, 10−11.
(2) Park, S.; Ruoff, R. S. Chemical Methods for the Production of Graphenes. *Nat. Nanotechnol.* **2009**, *4*, 217−224.
(3) Eigler, S.; Enzelberger-Heim, M.; Grimm, S.; Hofmann, P.; Kroener, W.; Geworski, A.; Dotzer, C.; Röckert, M.; Xiao, J.; Papp, C.; Lytken, O.; Steinrück, H. P.; Müller, P.; Hirsch, A. Wet Chemical Synthesis of Graphene. *Adv. Mater.* **2013**, *25*, 3583−3587.
(4) Gulia, P.; Brajpuriya, R.; Kumar, S.; Tripathi, A. Synthesis of Graphene Oxide Thin Film and Effect of Electron Beam Irradiation. *AIP Conf. Proc.* **2017**, DOI: 10.1063/1.4980805.
(5) Tung, T. T.; Yoo, J.; Alotaibi, F. K.; Nine, M. J.; Karunagaran, R.; Krebsz, M.; Nguyen, G. T.; Tran, D. N. H.; Feller, J. F.; Losic, D. Graphene Oxide-Assisted Liquid Phase Exfoliation of Graphite into Graphene for Highly Conductive Film and Electromechanical Sensors. *ACS Appl. Mater. Interfaces* **2016**, *8*, 16521−16532.
(6) Liu, W.; Speranza, G. Tuning the Oxygen Content of Reduced Graphene Oxide and Effects on Its Properties. *ACS Omega* **2021**, *6*, 6195−6205.
(7) Veerapandian, M.; Lee, M. H.; Krishnamoorthy, K.; Yun, K. Synthesis, Characterization and Electrochemical Properties of Functionalized Graphene Oxide. *Carbon* **2012**, *50*, 4228−4238.
(8) Georgakilas, V.; Tiwari, J. N.; Kemp, K. C.; Perman, J. A.; Bourlinos, A. B.; Kim, K. S.; Zboril, R. Noncovalent Functionalization of Graphene and Graphene Oxide for Energy Materials, Biosensing, Catalytic, and Biomedical Applications. *Chem. Rev.* **2016**, *116*, 5464−5519.
(9) Tortello, M.; Colonna, S.; Bernal, M.; Gomez, J.; Pavese, M.; Novara, C.; Giorgis, F.; Maggio, M.; Guerra, G.; Saracco, G.; Gonnelli, R. S.; Fina, A. Effect of Thermal Annealing on the Heat Transfer Properties of Reduced Graphite Oxide Flakes: A Nanoscale

Characterization via Scanning Thermal Microscopy. *Carbon* **2016**, *109*, 390−401.
(10) Huang, L.; Liu, Y.; Ji, L.-C.; Xie, Y.-Q.; Wang, T.; Shi, W.-Z. Pulsed Laser Assisted Reduction of Graphene Oxide. *Carbon* **2011**, *49*, 2431−2436.
(11) Loh, K. P.; Bao, Q.; Eda, G.; Chhowalla, M. Graphene Oxide as a Chemically Tunable Platform for Optical Applications. *Nat. Chem.* **2010**, *2*, 1015−1024.
(12) Wang, F. B.; Wang, J.; Shao, L.; Zhao, Y.; Xia, X. H. Hybrids of Gold Nanoparticles Highly Dispersed on Graphene for the Oxygen Reduction Reaction. *Electrochem. Commun.* **2014**, *38*, 82−85.
(13) Siklitskaya, A.; Gacka, E.; Larowska, D.; Mazurkiewicz-Pawlicka, M.; Malolepszy, A.; Stobiński, L.; Marciniak, B.; Lewandowska-Andrałojć, A.; Kubas, A. Lerf−Klinowski-Type Models of Graphene Oxide and Reduced Graphene Oxide Are Robust in Analyzing Non-Covalent Functionalization with Porphyrins. *Sci. Rep.* **2021**, *11*, 7977−7914.
(14) Hegde, M.; Yang, L.; Vita, F.; Fox, R. J.; van de Watering, R.; Norder, B.; Lafont, U.; Francescangeli, O.; Madsen, L. A.; Picken, S. J.; Samulski, E. T.; Dingemans, T. J. Strong Graphene Oxide Nanocomposites from Aqueous Hybrid Liquid Crystals. *Nat. Commun.* **2020**, *11*, 1−7.
(15) Zhao, G.; Qing, H.; Huang, G.; Genin, G. M.; Lu, T. J.; Luo, Z.; Xu, F.; Zhang, X. Reduced Graphene Oxide Functionalized Nanofibrous Silk Fibroin Matrices for Engineering Excitable Tissues. *NPG Asia Mater.* **2018**, *10*, 982−994.
(16) Tian, W.; Liu, X.; Yu, W. Research Progress of Gas Sensor Based on Graphene and Its Derivatives: A Review. *Appl. Sci.* **2018**, *8*, 1118.
(17) Kim, J.; Eum, J. H.; Kang, J.; Kwon, O.; Kim, H.; Kim, D. W. Tuning the Hierarchical Pore Structure of Graphene Oxide through Dual Thermal Activation for High-Performance Supercapacitor. *Sci. Rep.* **2021**, *11*, 2063−2010.
(18) Kashif, M.; Jafaar, E.; Sahari, S. K.; Low, F. W.; Hoa, N. D.; Ahmad, A.; Abbas, A.; Ngaini, Z.; Shafa, M.; Qurashi, A. Organic Sensitization of Graphene Oxide and Reduced Graphene Oxide Thin Films for Photovoltaic Applications. *Int. J. Energy Res.* **2021**, *45*, 9657−9666.
(19) Zheng, X.; Jia, B.; Chen, X.; Gu, M. In Situ Third-Order Non-Linear Responses during Laser Reduction of Graphene Oxide Thin Films towards on-Chip Non-Linear Photonic Devices. *Adv. Mater.* **2014**, *26*, 2699−2703.
(20) Bao, Q.; Zhang, H.; Wang, Y.; Ni, Z.; Yan, Y.; Shen, Z. X.; Loh, K. P.; Tang, D. Y. Atomic-Layer Graphene as a Saturable Absorber for Ultrafast Pulsed Lasers. *Adv. Funct. Mater.* **2009**, *19*, 3077−3083.
(21) Li, R.; Wang, Y.; Du, J.; Wang, X.; Duan, A.; Gao, R.; Liu, J.; Li, B. Graphene Oxide Loaded with Tumor-Targeted Peptide and Anti-Cancer Drugs for Cancer Target Therapy. *Sci. Rep.* **2021**, *11*, 1725−1710.
(22) Eigler, S.; Hirsch, A. Chemistry with Graphene and Graphene Oxide — Challenges for Synthetic Chemists. *Angew. Chem., Int. Ed.* **2014**, *53*, 7720−7738.
(23) Nebol, V. A.; Galstyan, V.; Silina, Y. E. Graphene Oxide and Its Chemical Nature : Multi-Stage Interactions between the Oxygen and Graphene. *Surf. Interfaces.* **2020**, *21*, 100763.
(24) Park, S.; An, J.; Jung, I.; Piner, R. D.; An, S. J.; Li, X.; Velamakanni, A.; Ruoff, R. S. Colloidal Suspensions of Highly Reduced Graphene Oxide in a Wide Variety of Organic Solvents. *Nano Lett.* **2009**, *9*, 1593−1597.
(25) Youn, S. C.; Geng, J.; Son, B. S.; Yang, S. B.; Kim, D. W.; Cho, H. M.; Jung, H. T. Effect of the Exposure Time of Hydrazine Vapor on the Reduction of Graphene Oxide Films. *J. Nanosci. Nanotechnol.* **2011**, *11*, 5959−5964.
(26) Guo, L.; Shao, R.-Q.; Zhang, Y.-L.; Jiang, H.-B.; Li, X.-B.; Xie, S.-Y.; Xu, B.-B.; Chen, Q.-D.; Song, J.-F.; Sun, H.-B. Bandgap Tailoring and Synchronous Microdevices Patterning of Graphene Oxides. *J. Phys. Chem. C* **2012**, *116*, 3595−3599.
(27) Chang, Y.-S.; Chen, F.-K.; Tsai, D.-C.; Kuo, B.-H.; Shieu, F.-S. N-Doped Reduced Graphene Oxide for Room-Temperature NO Gas Sensors. *Sci. Rep.* **2021**, *11*, 20719−20712.
(28) Torres, D.; Pinilla, J. L.; Moliner, R.; Suelves, I. On the Oxidation Degree of Few-Layer Graphene Oxide Sheets Obtained from Chemically Oxidized Multiwall Carbon Nanotubes. *Carbon* **2015**, *81*, 405−417.
(29) King, A. A. K.; Davies, B. R.; Noorbehesht, N.; Newman, P.; Church, T. L.; Harris, A. T.; Razal, J. M.; Minett, A. I. A New Raman Metric for the Characterisation of Graphene Oxide and Its Derivatives. *Sci. Rep.* **2016**, *6*, 19491−19496.
(30) Dahlberg, T. *The First Order Raman Spectrum of Isotope Labelled Nitrogen-Doped Reduced Graphene Oxide*; Umeå University: Sweden, 2016.
(31) Korepanov, V. I. Asymmetric Least-Squares Baseline Algorithm with Peak Screening for Automatic Processing of the Raman Spectra. *J. Raman Spectrosc.* **2020**, *51*, 2061−2065.
(32) Ferrari, A. C.; Robertson, J. Interpretation of Raman Spectra of Disordered and Amorphous Carbon. *Phys. Rev. B* **2000**, *61*, 14095−14107.
(33) Ferrari, A. C.; Basko, D. M. Raman Spectroscopy as a Versatile Tool for Studying the Properties of Graphene. *Nat. Nanotechnol.* **2013**, *8*, 235−246.
(34) Schwan, J.; Ulrich, S.; Batori, V.; Ehrhardt, H.; Silva, S. R. P. Raman Spectroscopy on Amorphous Carbon Films. *J. Appl. Phys.* **1996**, *80*, 440−447.
(35) Tan, P. H.; Deng, Y. M.; Zhao, Q. Temperature-Dependent Raman Spectra and Anomalous Raman Phenomenon of Highly Oriented Pyrolytic Graphite. *Condens. Matter Mater. Phys.* **1998**, *58*, 5435−5439.
(36) Jawhari, T.; Roid, A.; Casado, J. Raman Spectroscopic Characterization of Some Commercially Available Carbon Black Materials. *Carbon* **1995**, *33*, 1561−1565.
(37) Kaniyoor, A.; Ramaprabhu, S. A Raman Spectroscopic Investigation of Graphite Oxide Derived Graphene. *AIP Adv.* **2012**, *2*, 4600.
(38) Ferrari, A. C.; Robertson, J. Origin of the 1150 − Cm^{-1} Raman Mode in Nanocrystalline Diamond. *Phys. Rev. B: Condens. Matter Mater. Phys.* **2001**, *63*, 2−5.
(39) Wang, Y.; Alsmeyer, D. C.; McCreery, R. L. Raman Spectroscopy of Carbon Materials: Structural Basis of Observed Spectra. *Chem.Mater.* **1990**, *2*, 563−577.
(40) Sadezky, A.; Muckenhuber, H.; Grothe, H.; Niessner, R.; Pöschl, U. Raman Microspectroscopy of Soot and Related Carbonaceous Materials: Spectral Analysis and Structural Information. *Carbon* **2005**, *43*, 1731−1742.
(41) Scardaci, V.; Compagnini, G. Raman Spectroscopy Investigation of Graphene Oxide Reduction by Laser Scribing. *C* **2021**, *7*, 48.
(42) Zhu, P.; Shen, M.; Xiao, S.; Zhang, D. Experimental Study on the Reducibility of Graphene Oxide by Hydrazine Hydrate. *Phys. B* **2011**, *406*, 498−502.
(43) Lerf, A.; Buchsteiner, A.; Pieper, J.; Schöttl, S.; Dekany, I.; Szabo, T.; Boehm, H. P. Hydration Behavior and Dynamics of Water Molecules in Graphite Oxide. *J. Phys. Chem. Solids* **2006**, *67*, 1106−1110.
(44) Kravets, V. G.; Marshall, O. P.; Nair, R. R.; Thackray, B.; Zhukov, A.; Leng, J.; Grigorenko, A. N. Engineering Optical Properties of a Graphene Oxide Metamaterial Assembled in Microfluidic Channels. *Opt. Express* **2015**, *23*, 1265.
(45) Kumar, N.; Das, S.; Bernhard, C.; Varma, G. D. Effect of Graphene Oxide Doping on Superconducting Properties of Bulk MgB_2. *Supercond. Sci. Technol.* **2013**, *26*, No. 095008.
(46) Omidvar, A.; Rashidianvaziri, M. R.; Jaleh, B.; Partovi Shabestari, N.; Noroozi, M. Metal-Enhanced Fluorescence of Graphene Oxide by Palladium Nanoparticles in the Blue-Green Part of the Spectrum. *Chinese Phys. B* **2016**, *25*, 118102.
(47) Sharma, V.; Jain, Y.; Kumari, M.; Gupta, R.; Sharma, S. K.; Sachdev, K. Synthesis and Characterization of Graphene Oxide (GO)

https://doi.org/10.1021/acsomega.2c00108
ACS Omega 2022, 7, 11973−11979

and Reduced Graphene Oxide (RGO) for Gas Sensing Application. *Macromol. Symp.* **2017**, *376*, 1700006−1700005.
(48) Sinha, A.; Thakur, A. D. Experimental Bandgap Tuning of Graphene Oxide with Varying Degree of Oxidation and Reduction. *AIP Conf. Proc.* **2020**, *2220*, 140008.
(49) Zheng, F.; Xu, W. L.; Jin, H. D.; Hao, X. T.; Ghiggino, K. P. Charge Transfer from Poly(3-Hexylthiophene) to Graphene Oxide and Reduced Graphene Oxide. *RSC Adv.* **2015**, *5*, 89515−89520.
(50) Tauc, J.; Grigorovici, R.; Vancu, A. Optical Properties and Electronic Structure of Amorphous Germanium. *Phys. Status Solidi* **1966**, *15*, 627−637.
(51) Yu, P. Y.; Cardona, M. *Fundamentals of Semiconductors*; 3rd ed.;. Springer: Berlin Heidelberg New York, 2005.
(52) Dongol, M.; El-Denglawey, A.; Abd El Sadek, M. S.; Yahia, I. S. Thermal Annealing Effect on the Structural and the Optical Properties of Nano CdTe Films. *Optik.* **2015**, *126*, 1352−1357.
(53) El-Denglawey, A.; Makhlouf, M. M.; Dongol, M. Physical Aging Effects on the Structural and Optical Properties of Nano As-Se-Tl Films. *J. Non-Cryst. Solids* **2016**, *449*, 34−40.
(54) Zhang, Q.; Zhang, H.; Cheng, X. L. Highly Stable Two-Dimensional Graphene Oxide: Electronic Properties of Its Periodic Structure and Optical Properties of Its Nanostructures. *Chinese Phys. B* **2018**, *27*, No. 027301.
(55) Lundie, M.; Šljivančanin, Ž.; Tomić, S. Electronic and Optical Properties of Reduced Graphene Oxide. *J. Mater. Chem. C* **2015**, *3*, 7632−7641.
(56) De Silva, K. K. H.; Viswanath, P.; Rao, V. K.; Suzuki, S.; Yoshimura, M. New Insight into the Characterization of Graphene Oxide and Reduced Graphene Oxide Monolayer Flakes on Si-Based Substrates by Optical Microscopy and Raman Spectroscopy. *J. Phys. Chem. C* **2021**, *125*, 7791−7798.
(57) Buchsteiner, A.; Lerf, A.; Pieper, J. Water Dynamics in Graphite Oxide Investigated with Neutron Scattering. *J. Phys. Chem. B* **2006**, *110*, 22328−22338.
(58) Talyzin, A. V.; Hausmaninger, T.; You, S.; Szabó, T. The Structure of Graphene Oxide Membranes in Liquid Water, Ethanol and Water-Ethanol Mixtures. *Nanoscale* **2014**, *6*, 272−281.
(59) Moon, I. K.; Lee, J.; Ruoff, R. S.; Lee, H. Reduced Graphene Oxide by Chemical Graphitization. *Nat. Commun.* **2010**, *1*, 73.
(60) Çaldiran, Z.; Şinoforoğlu, M.; Metin, Ö.; Aydoğan, Ş.; Meral, K. Space Charge Limited Current Mechanism (SCLC) in the Graphene Oxide-Fe_3O_4 Nanocomposites/n-Si Heterojunctions. *J. Alloys Compd.* **2015**, *631*, 261−265.
(61) Venugopal, G.; Krishnamoorthy, K.; Mohan, R.; Kim, S. J. An Investigation of the Electrical Transport Properties of Graphene-Oxide Thin Films. *Mater. Chem. Phys.* **2012**, *132*, 29−33.
(62) Montgomery, H. C. Method for Measuring Electrical Resistivity of Anisotropic Materials. *J. Appl. Phys.* **1971**, *42*, 2971.
(63) Liu, F.; Cao, Y.; Yi, M.; Xie, L.; Huang, W.; Tang, N.; Zhong, W.; Du, Y. Thermostability, Photoluminescence, and Electrical Properties of Reduced Graphene Oxide-Carbon Nanotube Hybrid Materials. *Crystals* **2013**, *3*, 28−37.
(64) Choi, S. J.; Kim, S. J.; Kim, I. D. Ultrafast Optical Reduction of Graphene Oxide Sheets on Colorless Polyimide Film for Wearable Chemical Sensors. *NPG Asia Mater.* **2016**, *8*, No. e315.
(65) Golan, G.; Axelevitch, A.; Gorenstein, B.; Manevych, V. Hot-Probe Method for Evaluation of Impurities Concentration in Semiconductors. 2006, *37* (9), 910−915, DOI: 10.1016/j.mejo.2006.01.014.

Recommended by ACS

Modification of Graphene Oxide/V2O5·nH2O Nanocomposite Films via Direct Laser Irradiation
Algirdas Lazauskas, Mindaugas Andrulevicius, *et al.*
APRIL 06, 2020
ACS APPLIED MATERIALS & INTERFACES
READ

Enhanced Nonlinear Saturable Absorption of MoS2/Graphene Nanocomposite Films
Minmin He, Xinlong Xu, *et al.*
NOVEMBER 09, 2017
THE JOURNAL OF PHYSICAL CHEMISTRY C
READ

Synthesis of Silanized MoS2/Reduced Graphene Oxide for Strong Radar Wave Absorption
Jing Ran, Heqing Fu, *et al.*
AUGUST 31, 2017
INDUSTRIAL & ENGINEERING CHEMISTRY RESEARCH
READ

Solution-Processed Natural Konjac Glucomannan Material for Resistive Switching Memory
Yu-Chi Chang, Ya Lan Hsu, *et al.*
DECEMBER 29, 2021
ACS APPLIED ELECTRONIC MATERIALS
READ

Get More Suggestions >

https://doi.org/10.1021/acsomega.2c00108
ACS Omega 2022, 7, 11973−11979